Moving Element Analysis of High-Speed Train-Slab Track System Considering Discrete Rail Pads

Tuo Lei
School of Civil Engineering, Chang'an University, Xi'an 710061, China
Leituo616@163.com

Jian Dai*
Department of Marine Technology
Norwegian University of Science and Technology, Trondheim NO-7491, Norway
**jian.dai@ntnu.no*

KoK Keng Ang
Department of Civil and Environmental Engineering
National University of Singapore, Singapore 117576, Singapore
kk_ang@nus.edu.sg

Kun Li and Yi Liu
School of Civil Engineering, Chang'an University, Xi'an 710061, China
2435936232@qq.com, 17319597785@163.com

Received (5 May 2020)
Accepted (Day Month 2020)

This paper presents a study of the dynamic behavior of a coupled train-slab track system considering discrete rail pads. The slab track is modelled as a three-layer Timoshenko beam. The study is carried out using the moving element method (MEM). By introducing a convected coordinate system moving at the same speed as the vehicle, the governing equations of motion of the slab track are formulated in a moving frame-of-reference. By adopting the Galerkin's method, the element stiffness, mass and damping matrices of a truncated slab track in the moving coordinate system are derived. The vehicle is modelled as a multi-body with 10 degrees of freedom. The nonlinear Hertz contact model is used to account for the wheel-rail interaction. The Newmark integration method, in conjunction with a global Newton-Raphson iteration algorithm, is employed to solve the nonlinear dynamic equations of motion of the vehicle-track coupled system. The proposed MEM model of the system is validated through comparison with available results in the literature. Further study is then made to investigate the vehicle-track system accounting for track irregularities modelled as short harmonic wave forms. Results showed that irregularities with short wavelengths have a significant effect on wheel-rail contact force and rail acceleration, and the dynamic response of the track structure does not increase monotonously with the increase of the vehicle speed.

Keywords: Slab track; Timoshenko beam; moving element method; discrete rail pads; dynamics.

*Corresponding author.

1. Introduction

Since China's first high-speed rail line (Beijing-Tianjin intercity railway) was completed in 2008, China's high-speed rail mileage had reached 29,000 kilometers in the past 10 years by 2018 and ranked the first in the world. In terms of the form of track designs, the slab (ballastless) track has become the most used design for the construction of high-speed rails in China. Compared to the traditional ballasted track, the slab track is a modern design that was developed and employed in the Japanese Shinkansen high-speed railway in the 1960s. The rapid development and wide adoption of the slab track can be attributed to its higher running stability, better stiffness uniformity and lower maintenance cost than the ballasted track.[1,2] To continuously improve the safety and comfort of high-speed trains and extend their service life, the dynamic behavior of a railway track has been a focus for research and study globally.

Historically, early models of the train-track system treated vehicles as moving loads and tracks as infinitely long beams on elastic foundations. Based on these models, many analytical approaches including the Laplace transform method,[3] Fourier transform,[4] Fast Fourier transform,[5] mode superposition,[6] and spectral element method[7] have been used to solve the governing equations of motion of the system. However, these analytical solutions are often limited to linear elastic assumptions and greatly simplified applications. These approaches are inadequate in dealing with today's complex railway problems.

The finite element method (FEM) is a powerful numerical approach for structural analysis and has been widely used to solve various train-track problems. Filho[8] presented a review on the use of the FEM in solving the problem of a uniform beam subject to a moving load. Esmaeili et al.[9] modelled the slab track as a double Euler-Bernoulli beam, developed a vehicle-slab track interaction algorithm for the dynamic simulation of the coupled vehicle-track system and analyzed the effects of the slab thickness, foundation stiffness and axle load on dynamic responses of the system. Lei and Zhang[10] proposed a slab track element model with a three-layer Euler-Bernoulli beam and a vehicle element model with 26 degrees of freedom. A direct integration scheme was employed to calculate the dynamic response of the coupled vehicle-track system. Zhai et al.[11] further improved the slab track model by considering two parallel continuous beams supported by a series of elastic plates on a viscoelastic foundation. The vehicle and track subsystems were coupled through a wheel-rail model that accounts for the three-dimensional vibrations of the rails. Moreover, a fast explicit integration method was applied to solve the nonlinear equations of motion of the system in the time domain. Xu et al.[12] established a three-dimensional coupled vehicle-slab track-subgrade finite element model. The dynamic characteristics and the corresponding dynamic coefficient of slab track system were studied considering different types of track irregularity.

From the existing literature, it may be concluded that there are mainly three types of finite element models, namely the multi-layer beam model, beam-slab model and beam-solid element model, that can be used for the dynamic analysis of the coupled train and slab track system. However, since the track degradation mainly occurs in the vertical direction[13] and for the sake of computational efficiency, the multi-layer beam model is still one of the most widely used models. In a conventional FEM model, a global fixed coordinate system is used to formulate the structural matrices. As the vehicle moves from one track element to the next, the loads vector must be updated at each time step for tracking the position of moving wheels. A refined mesh is usually needed to ensure a satisfactory degree of accuracy of the results. In addition, a large domain size is often required for the simulations, especially when the speed of the vehicle is high. These disadvantages make the FEM computationally inefficient for analyzing coupled high-speed train-track systems.

To overcome the abovementioned complications faced by the FEM, Krenk et al.[14] proposed the use of FEM involving a moving coordinate to study the wave propagation problem of an elastic half space subject to a moving load. By using a Galilean coordinate transformation, Andersen et al.[15] derived the FEM formulation of an infinite Euler beam resting on a linear viscoelastic Kelvin foundation subject to a harmonic moving load. In their study, the equations of motion of the beam under the moving load were formulated in a convected coordinate system that travels with the moving load. Subsequently, Koh et al.[16] studied dynamic responses of a coupled train-track system in a moving coordinate system and termed the approach the moving element method (MEM). By discretizing the truncated track model into elements that 'flow' with the same speed as the moving vehicle, the vehicle load is always 'stationary' in the moving frame-of-reference. This method not only eliminates the need to track and update wheel positions but also ensures that the vehicle in question would never move out of the finite model. Since then, many researchers have applied this technique to study various moving load problems.[17-28] For example, Ang and Dai[17] employed the MEM to investigate the dynamic response of a high-speed rail system accounting for an abrupt change of the foundation stiffness. The railway beam was treated as a viscously damped Euler-Bernoulli beam resting on a Winkler foundation. By employing a two-parameter Pasternak foundation model, Tran et al.[18] studied the dynamic response of a high-speed train subject to abrupt braking. More recently, the liquid sloshing behavior and its effect on the braking of a partially filled freight train were examined.[19] A computational scheme was proposed by Dai et al.[20] in conjunction with the MEM to study the dynamic responses of a coupled high-speed train-train system accounting for the effect of periodically placed discrete supports beneath the rail beam. Subsequently, Dai et al.[21] modelled the ballasted track in a moving coordinate system by using a three-layer model consisting of a continuous rail, discrete sleepers and ballast, and studied the dynamic response of a high-speed train-track system considering unsupported sleepers. Lei and Wang[22] developed a slab track element model with a three-layer Euler-Bernoulli beam system to investigate the dynamic behavior of the coupled train-slab track system. In their study, the effect of discrete rail pads and the nonlinear relationship of wheel-rail contact were neglected. It should be noted that in real situations, the rail may not resemble a slender beam due to the short spacing (usually 600-650 mm) between adjacent supports. Studies have shown that the shear-deformable Timoshenko beam model is superior to the classic Euler-Bernoulli model in describing the rail vibrations especially in the high frequency range.[29-31] Therefore, it is important that the slab tracks are properly modelled to ensure a realistic analysis of the high-speed train-track system.

In this paper, a computational model in conjunction with the MEM is proposed to study the dynamic response of a coupled high-speed train-slab track system. A new slab track model comprising a three-layer Timoshenko beam supported by discrete rail pads and sustaining substructures is presented. The accuracy of the proposed computational model is evaluated by comparison with available results in the literature. The effects of track irregularities and vehicle speeds on the dynamic response of the coupled train-track system are examined and discussed.

2. Fundamental Assumptions

The following assumptions are made as a basis for establishing the mathematical model of the vehicle-slab track system:

(1) Only the vertical dynamic responses are of concern in this study.

(2) Half of the vehicle-slab track system is modelled in view that the system is symmetrical about the centerline in the longitudinal direction.

(3) The vehicle model is based on the CHR3[32] locomotive unit with primary and secondary suspension systems, in which the vertical and pitch motions of the coach body and bogies are considered.

(4) The track system is based on the CRTSII[32] slab track consisting of the rail beam, rail pads, track slab, cement asphalt (CA) mortar layer, concrete base and subgrade.

(5) The rail is treated as an infinitely long elastic beam supported by discrete pads with elastic stiffness and damping properties.

(6) The track slab and concrete base are idealized as elastic beams supported by continuous CA mortar and subgrade, respectively. Only the elastic stiffness and damping properties of the CA mortar and subgrade are considered.

3. Mathematical Formulation

The vehicle-slab track system comprises two parts. The first corresponds to the vehicle which includes the coach body, bogies and wheel-sets. The second is composed of the rail and supporting structures. The schematic drawing of the coupled system is shown in Fig. 1, in which the vehicle is modelled as a multi-body system with 10 degrees of freedom (DOFs), and the slab track is represented by a three-layer Timoshenko beam model. The vehicle is assumed to move at a constant speed V in the positive x-direction. Note that in the employed coordinate system, the vertical displacement and force are positive in the upward direction and the rotation and moment are positive in the counterclockwise direction.

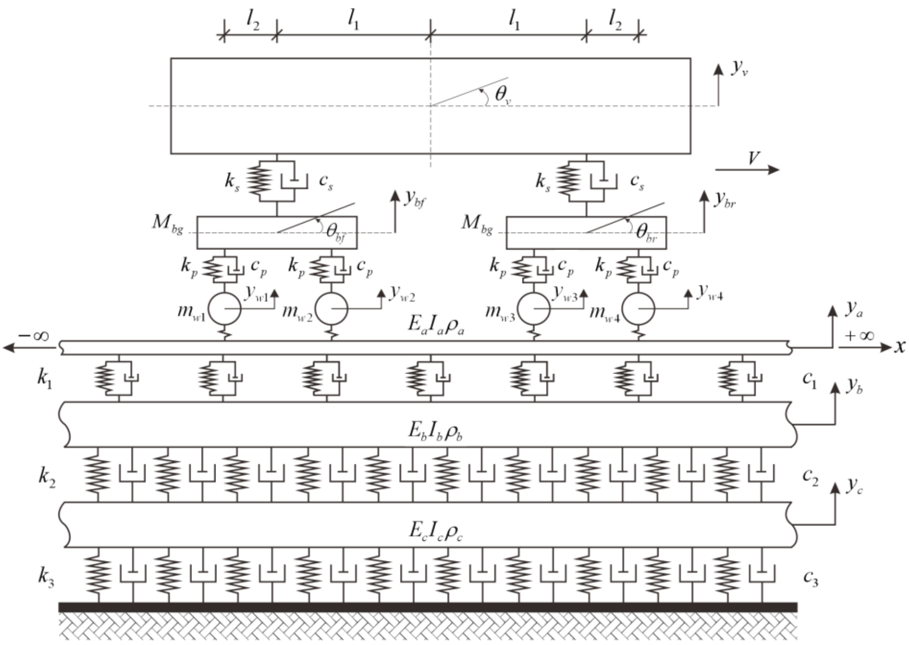

Fig. 1. Vehicle-slab track system.

3.1. *Slab track model*

The slab track model comprises three Timoshenko beams representing the rail, track slab and concrete base, respectively. These are interconnected by spring-dashpot units (refer to Fig. 1). The densities of the rail, track slab and concrete base are labelled as ρ_a, ρ_b and ρ_c respectively. Likewise, their cross-sectional areas are denoted as A_a, A_b and A_c; the second moments of area are I_a, I_b and I_c; the Young's moduli are E_a, E_b and E_c; the shear moduli are G_a, G_b and G_c; and the Timoshenko shear correction coefficients are k_a, k_b and k_c, respectively.

The rail is supported by a layer of evenly spaced rail pads with stiffness coefficient k_1 and damping coefficient c_1. Using the same method employed by Dai et al[21] and Lei and Wang[22] , the vertical force and moment dynamic equilibrium of an infinitesimal part of the rail of length dx can be established using d'Alembert's principle. The two coupled second-order differential equations of the coupled rail-track slab can be written as

$$\rho_a A_a \frac{\partial^2 y_a(x,t)}{\partial t^2} - k_a A_a G_a \frac{\partial^2 y_a(x,t)}{\partial x^2} + k_a A_a G_a \frac{\partial \varphi_a(x,t)}{\partial x} + \sum_{i=1}^{n} c_1 \left(\frac{\partial y_a(x,t)}{\partial t} - \frac{\partial y_b(x,t)}{\partial t} \right) \tag{1}$$
$$\times \delta(x - iL_s) + \sum_{i=1}^{n} k_1 \left(y_a(x,t) - y_b(x,t) \right) \times \delta(x - iL_s) = -\sum_{j=1}^{m} F_j \delta\left(x - X_j(t)\right),$$

$$\rho_a I_a \frac{\partial^2 \varphi_a(x,t)}{\partial t^2} - E_a I_a \frac{\partial^2 \varphi_a(x,t)}{\partial x^2} - k_a A_a G_a \frac{\partial y_a(x,t)}{\partial x} + k_a A_a G_a \varphi_a(x,t) = 0, \tag{2}$$

where y_a and y_b denote the vertical displacements of the rail beam and track slab, respectively, and φ_a the bending rotation of the rail. The contact force between the j th wheel-set and rail is denoted by F_j ($j=1,2,3,4$). Other notaions used are L_s the spacing between two adjacent pads along the track, X_j the travel distance of the j th wheel-set and $\delta(\bullet)$ the Dirac-delta function.

For the track slab supported by the CA mortar with stiffness k_2 and damping coefficient c_2, the equations of motion are given by

$$\begin{aligned}
&\rho_b A_b \frac{\partial^2 y_b(x,t)}{\partial t^2} - k_b A_b G_b \frac{\partial^2 y_b(x,t)}{\partial x^2} + k_b A_b G_b \frac{\partial \varphi_b(x,t)}{\partial x} + \sum_{i=1}^{n} c_1 \left(\frac{\partial y_b(x,t)}{\partial t} - \frac{\partial y_a(x,t)}{\partial t} \right) \\
&\quad \times \delta(x - iL_s) + \sum_{i=1}^{n} k_1 \left(y_b(x,t) - y_a(x,t) \right) \times \delta(x - iL_s) + c_2 \left(\frac{\partial y_b(x,t)}{\partial t} - \frac{\partial y_c(x,t)}{\partial t} \right) \\
&\quad + k_2 \left(y_b(x,t) - y_c(x,t) \right) = 0,
\end{aligned} \tag{3}$$

$$\rho_b I_b \frac{\partial^2 \varphi_b(x,t)}{\partial t^2} - E_b I_b \frac{\partial^2 \varphi_b(x,t)}{\partial x^2} - k_b A_b G_b \frac{\partial y_b(x,t)}{\partial x} + k_b A_b G_b \varphi_b(x,t) = 0, \tag{4}$$

where y_c denotes the displacement of the concrete base, and φ_b the bending rotation of the track slab.

Similarly, for the concrete base supported by the subgrade with stiffness k_3 and damping coefficient c_3, the equations of motion are given by

$$\begin{aligned}
&\rho_c A_c \frac{\partial^2 y_c(x,t)}{\partial t^2} - k_c A_c G_c \frac{\partial^2 y_c(x,t)}{\partial x^2} + k_c A_c G_c \frac{\partial \varphi_c(x,t)}{\partial x} + c_2 \left(\frac{\partial y_c(x,t)}{\partial t} - \frac{\partial y_b(x,t)}{\partial t} \right) \\
&\quad + k_2 \left(y_c(x,t) - y_b(x,t) \right) + c_3 \frac{\partial y_c(x,t)}{\partial t} + k_3 y_c(x,t) = 0,
\end{aligned} \tag{5}$$

$$\rho_c I_c \frac{\partial^2 \varphi_c(x,t)}{\partial t^2} - E_c I_c \frac{\partial^2 \varphi_c(x,t)}{\partial x^2} - k_c A_c G_c \frac{\partial y_c(x,t)}{\partial x} + k_c A_c G_c \varphi_c(x,t) = 0, \tag{6}$$

where φ_c denotes the bending rotation of the concrete base.

3.2. *Vehicle model*

The 10-DOF vehicle model is composed of a coach body with two bogies and four wheel-sets, as illustrated in Fig. 1. The coach body has a lumped mass m_v and moment of inertia J_v. The two bogies have an identical lumped mass m_{bg} and moment of inertia J_b. Each of the four wheel-sets has a lumped mass $m_{wj}(j=1,2,3,4)$. According to Newton's second law of motion, the governing equations of the vehicle can be written as

$$m_v \ddot{y}_v + c_s(2\dot{y}_v - \dot{y}_{br} - \dot{y}_{bf}) + k_s(2y_v - y_{br} - y_{bf}) = -m_c g, \tag{7}$$

$$J_v \ddot{\theta}_v + c_s l_1(\dot{y}_{br} + 2\dot{\theta}_v l_1 - \dot{y}_{bf}) + k_s l_1(y_{br} + 2\theta_v l_1 - y_{bf}) = 0, \tag{8}$$

$$m_{bg}\ddot{y}_{br}+c_s(\dot{y}_{br}+\dot{\theta}_v l_1-\dot{y}_v)+c_p(2\dot{y}_{br}-\dot{y}_{w1}-\dot{y}_{w2})+k_s(y_{br}+\theta_v l_1-y_v) \\ +k_p(2y_{br}-y_{w1}-y_{w2})=-m_{bg}g, \tag{9}$$

$$J_b\ddot{\theta}_{br}+c_p l_2(\dot{y}_{w1}+2\dot{\theta}_{br}l_2-\dot{y}_{w2})+k_p l_2(y_{w1}+2\theta_{br}l_2-y_{w2})=0, \tag{10}$$

$$m_{bg}\ddot{y}_{bf}+c_s(\dot{y}_{bf}-\dot{\theta}_v l_1-\dot{y}_v)+c_p(2\dot{y}_{bf}-\dot{y}_{w3}-\dot{y}_{w4})+k_s(y_{bf}-\theta_v l_1-y_v) \\ +k_p(2y_{bf}-y_{w3}-y_{w4})=-m_{bg}g, \tag{11}$$

$$J_b\ddot{\theta}_{bf}+c_p l_2(\dot{y}_{w3}+2\dot{\theta}_{bf}l_2-\dot{y}_{w4})+k_p l_2(y_{w3}+2\theta_{bf}l_2-y_{w4})=0, \tag{12}$$

$$m_{w1}\ddot{y}_{w1}+c_p(\dot{y}_{w1}+\dot{\theta}_{br}l_2-\dot{y}_{br})+k_p(y_{w1}+\theta_{br}l_2-y_{br})=F_1-m_{w1}g, \tag{13}$$

$$m_{w2}\ddot{y}_{w2}+c_p(\dot{y}_{w2}-\dot{\theta}_{br}l_2-\dot{y}_{br})+k_p(y_{w2}-\theta_{br}l_2-y_{br})=F_2-m_{w2}g, \tag{14}$$

$$m_{w3}\ddot{y}_{w3}+c_p(\dot{y}_{w3}+\dot{\theta}_{bf}l_2-\dot{y}_{bf})+k_p(y_{w3}+\theta_{bf}l_2-y_{bf})=F_3-m_{w3}g, \tag{15}$$

$$m_{w4}\ddot{y}_{w4}+c_p(\dot{y}_{w4}-\dot{\theta}_{bf}l_2-\dot{y}_{bf})+k_p(y_{w4}-\theta_{bf}l_2-y_{bf})=F_4-m_{w4}g, \tag{16}$$

where y_v, y_{br}, y_{bf}, and y_{wj} ($j=1,2,3,4$) denote the vertical displacements at the centroids of the coach body, rear bogie, front bogie and wheel-sets, respectively. The pitching rotations at the centroids of the vehicle, rear bogie, and front bogie are denoted by θ_v, θ_{br}, and θ_{bf}, respectively; k_p and c_p denote the stiffness and damping coefficients of the primary suspension system; k_s and c_s are the corresponding coefficients of the secondary suspension system; $2l_1$ is the distance between two bogie centers; and $2l_2$ is the distance between the centers of two adjacent wheel-sets under the same bogie.

From Eqs. (7)-(16), the equation of motion of the moving vehicle can be written as

$$\mathbf{M}_U\ddot{\mathbf{Z}}_U+\mathbf{C}_U\dot{\mathbf{Z}}_U+\mathbf{K}_U\mathbf{Z}_U=\mathbf{F}_U, \tag{17}$$

where $\mathbf{M}_U$, $\mathbf{C}_U$ and $\mathbf{K}_U$ are the total mass, damping and stiffness matrices of the vehicle, respectively; $\mathbf{Z}_U$ and $\mathbf{F}_U$ the displacement and force vectors of the vehicle, respectively.

3.3. *Wheel-rail contact model*

The nonlinear Hertz contact model is adopted here for the computation of the normal contact force between the wheel and railhead. The contact force is given by Zhai[33] as

$$F_j=\left\{\begin{matrix}\left[\frac{1}{G}\left(y_{aj}+y_t-y_{wj}\right)\right]^{\frac{3}{2}} & y_{aj}+y_t-y_{wj}\geq 0 \\ 0 & y_{aj}+y_t-y_{wj}<0\end{matrix}\right\}, \tag{18}$$

where F_j denotes the Hertz normal contact force between the jth wheel-set and rail at the contact point; G is the wheel-rail contact coefficient (unit: $\mathrm{m/N^{2/3}}$) for the wheel with cone tread or worn tread. G can be chosen as $4.57R^{-0.149}\times 10^{-8}$ or $3.86R^{-0.115}\times 10^{-8}$, respectively, where R is the radius of the wheel, unit: m); y_{aj} is the displacement of the track at the contact point; y_t is the magnitude of track surface irregularity; and y_{wj} is the displacement of the jth wheel in contact with the rail.

4. Moving Element Method

The moving element method (MEM) involves the use of a moving coordinate *r*-axis (refer to Fig. 1) , whose relationship with the fixed *x*-axis is given by

$$r = x - Vt, \tag{19}$$

where the origin of the x-axis is located at the midpoint of the truncated track of length *L* and *V* is the velocity of the vehicle. The position of the track is within the interval $[-L/2, L/2]$ at time $t=0$ in the x-axis, which changes to $[Vt-L/2, Vt+L/2]$ at time *t*. When using a moving *r*-coordinate as defined in Eq. (19), the position of the track is always the interval $[-L/2, L/2]$ in the r-coordinate.

With the simple transformation,[16] the governing equations of the rail beam expressed in Eqs. (1) and (2) can be rewritten in the moving *r*-axis as

$$\begin{aligned}&\rho_a A_a\left(V^2\frac{\partial^2 y_a}{\partial r^2}-2V\frac{\partial y_a}{\partial r\partial t}+\frac{\partial^2 y_a}{\partial t^2}\right)-k_a A_a G_a\frac{\partial^2 y_a}{\partial r^2}+k_a A_a G_a\frac{\partial \varphi_a}{\partial r}\\&+\sum_{i=1}^{n}c_1\left(\frac{\partial y_a}{\partial t}-V\frac{\partial y_a}{\partial r}-\frac{\partial y_b}{\partial t}+V\frac{\partial y_b}{\partial r}\right)\times\delta(r+Vt-iL_s)\\&+\sum_{i=1}^{n}k_1\left(y_a-y_b\right)\times\delta(r+Vt-iL_s)=-\sum_{j=1}^{m}F_j\delta\left(r-R_j\right),\end{aligned}\tag{20}$$

$$\rho_a I_a\left(V^2\frac{\partial^2\varphi_a}{\partial r^2}-2V\frac{\partial\varphi_a}{\partial r\partial t}+\frac{\partial^2\varphi_a}{\partial t^2}\right)-E_a I_a\frac{\partial^2\varphi_a}{\partial r^2}-k_a A_a G_a\frac{\partial y_a}{\partial r}+k_a A_a G_a\varphi_a=0,\tag{21}$$

Similarly, Eqs. (3) - (6) can be rewritten as

$$\begin{aligned}&\rho_b A_b\left(V^2\frac{\partial^2 y_b}{\partial r^2}-2V\frac{\partial^2 y_b}{\partial r\partial t}+\frac{\partial^2 y_b}{\partial t^2}\right)-k_b A_b G_b\frac{\partial^2 y_b}{\partial r^2}+k_b A_b G_b\frac{\partial \varphi_b}{\partial r}\\&+\sum_{i=1}^{n}c_1\left(\frac{\partial y_b}{\partial t}-V\frac{\partial y_b}{\partial r}-\frac{\partial y_a}{\partial t}+V\frac{\partial y_a}{\partial r}\right)\times\delta(r+Vt-iL_s)\\&+\sum_{i=1}^{n}k_1\left(y_b-y_a\right)\times\delta(r+Vt-iL_s)+c_2\left(\frac{\partial y_b}{\partial t}-V\frac{\partial y_b}{\partial r}-\frac{\partial y_c}{\partial t}+V\frac{\partial y_c}{\partial r}\right)\\&+k_2\left(y_b-y_c\right)=0,\end{aligned}\tag{22}$$

$$\rho_b I_b\left(V^2\frac{\partial^2\varphi_b}{\partial r^2}-2V\frac{\partial^2\varphi_b}{\partial r\partial t}+\frac{\partial^2\varphi_b}{\partial t^2}\right)-E_b I_b\frac{\partial^2\varphi_b}{\partial r^2}-k_b A_b G_b\frac{\partial y_b}{\partial r}+k_b A_b G_b\varphi_b=0,\tag{23}$$

$$\rho_c A_c \left(V^2 \frac{\partial^2 y_c}{\partial r^2} - 2V \frac{\partial^2 y_c}{\partial r \partial t} + \frac{\partial^2 y_c}{\partial t^2} \right) - k_c A_c G_c \frac{\partial^2 y_c}{\partial r^2} + k_c A_c G_c \frac{\partial \varphi_c}{\partial r}$$
$$+ c_2 \left(\frac{\partial y_c}{\partial t} - V \frac{\partial y_c}{\partial r} - \frac{\partial y_b}{\partial t} + V \frac{\partial y_b}{\partial r} \right) + k_2 \left(y_c - y_b \right) + c_3 \left(\frac{\partial y_c}{\partial t} - V \frac{\partial y_c}{\partial r} \right) + k_3 y_c = 0, \tag{24}$$

$$\rho_c I_c \left(V^2 \frac{\partial^2 \varphi_c}{\partial r^2} - 2V \frac{\partial^2 \varphi_c}{\partial r \partial t} + \frac{\partial^2 \varphi_c}{\partial t^2} \right) - E_c I_c \frac{\partial^2 \varphi_c}{\partial r^2} - k_c A_c G_c \frac{\partial y_c}{\partial r} + k_c A_c G_c \varphi_c = 0. \tag{25}$$

To derive the moving element matrices of the track, a 6-node track element consisting of a three-layer beam element in the moving coordinate is established, as shown in Fig. 2. Note that y_a^i , φ_a^i and y_a^j , φ_a^j are the vertical displacements and bending rotations of the rail element at node 1 and node 4, respectively. Likewise, y_b^i , φ_b^i , y_b^j and φ_b^j correspond to nodes 2 and 5 of the track slab element; and y_c^i , φ_c^i , y_c^j and φ_c^j are for nodes 3 and 6 of the concrete base element. In this model, the rail pads are treated as discrete viscoelastic supports,[20] but the elastic stiffness and damping properties of the CA mortar and subgrade are modelled by using continuous viscoelastic spring-dashpot units. It is worth noting that when discrete rail pads are accounted for, the support stiffness of the rail always varies periodically with time in the moving coordinate and therefore needs to be constantly updated. So this moving element is different from the case of a continuously supported moving element employed by Lei and Wang.[22]

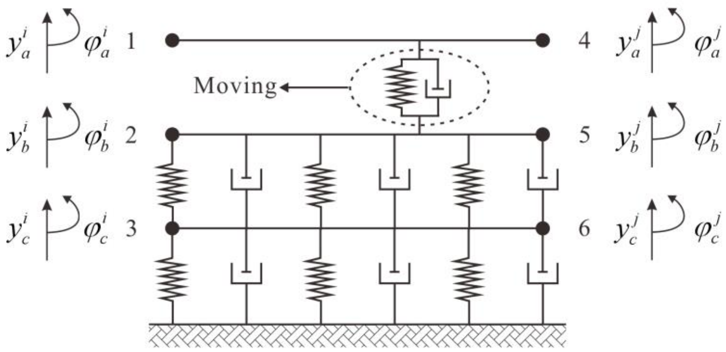

Fig. 2. Sketch of moving track element.

The nodal displacement vector of one typical moving track element can be written as

$$\mathbf{y}^e = \left\{ y_a^i \quad \varphi_a^i \quad y_b^i \quad \varphi_b^i \quad y_c^i \quad \varphi_c^i \quad y_a^j \quad \varphi_a^j \quad y_b^j \quad \varphi_b^j \quad y_c^j \quad \varphi_c^j \right\}^{\mathrm{T}}. \tag{26}$$

By introducing the interpolation functions, the displacements and bending rotations of the rail, track slab and concrete base within the moving element can be expressed as

$$y_a = \mathbf{N}_{ay} \mathbf{y}^e, y_b = \mathbf{N}_{by} \mathbf{y}^e, y_c = \mathbf{N}_{cy} \mathbf{y}^e, \tag{27}$$

$$\varphi_a = \mathbf{N}_{a\varphi} \mathbf{y}^e, \varphi_b = \mathbf{N}_{b\varphi} \mathbf{y}^e, \varphi_c = \mathbf{N}_{c\varphi} \mathbf{y}^e, \tag{28}$$

$$\mathbf{N}_{ay} = \left[N_{y1} \quad N_{y2} \quad 0 \quad 0 \quad 0 \quad 0 \quad N_{y3} \quad N_{y4} \quad 0 \quad 0 \quad 0 \quad 0 \right], \tag{29}$$

$$\mathbf{N}_{a\varphi} = \begin{bmatrix} N_{\varphi 1} & N_{\varphi 2} & 0 & 0 & 0 & 0 & N_{\varphi 3} & N_{\varphi 4} & 0 & 0 & 0 & 0 \end{bmatrix}, \tag{30}$$

$$\mathbf{N}_{by} = \begin{bmatrix} 0 & 0 & N_{y1} & N_{y2} & 0 & 0 & 0 & 0 & N_{y3} & N_{y4} & 0 & 0 \end{bmatrix}, \tag{31}$$

$$\mathbf{N}_{b\varphi} = \begin{bmatrix} 0 & 0 & N_{\varphi 1} & N_{\varphi 2} & 0 & 0 & 0 & 0 & N_{\varphi 3} & N_{\varphi 4} & 0 & 0 \end{bmatrix}, \tag{32}$$

$$\mathbf{N}_{cy} = \begin{bmatrix} 0 & 0 & 0 & 0 & N_{y1} & N_{y2} & 0 & 0 & 0 & 0 & N_{y3} & N_{y4} \end{bmatrix}, \tag{33}$$

$$\mathbf{N}_{c\varphi} = \begin{bmatrix} 0 & 0 & 0 & 0 & N_{\varphi 1} & N_{\varphi 2} & 0 & 0 & 0 & 0 & N_{\varphi 3} & N_{\varphi 4} \end{bmatrix}, \tag{34}$$

where, $\mathbf{N}_{ay}$, $\mathbf{N}_{by}$, $\mathbf{N}_{cy}$ and $\mathbf{N}_{a\varphi}$, $\mathbf{N}_{b\varphi}$, $\mathbf{N}_{c\varphi}$ denote the vectors of shape function for the vertical nodal displacements and bending rotations, respectively. The super convergent locking-free interdependent interpolation elements with cubic polynomial shape functions N_{yj} and $N_{\varphi j}$ (j = 1,2,3,4) proposed by Reddy[34] are employed.

Eqs. (20) and (21) are multiplied by a weighting function W and then integrated over a typical element length l, leading to the following weak form

$$\begin{aligned} \int_0^l W(r) \Bigg\{ & \rho_a A_a \left(V^2 \frac{\partial^2 y_a}{\partial r^2} - 2V \frac{\partial y_a}{\partial r \partial t} + \frac{\partial^2 y_a}{\partial t^2} \right) - k_a A_a G_a \frac{\partial^2 y_a}{\partial r^2} + k_a A_a G_a \frac{\partial \varphi_a}{\partial r} \\ & + \sum_{i=1}^{n} c_1 \left(\frac{\partial y_a}{\partial t} - V \frac{\partial y_a}{\partial r} - \frac{\partial y_b}{\partial t} + V \frac{\partial y_b}{\partial r} \right) \times \delta(r + Vt - iL_s) \\ & + \sum_{i=1}^{n} k_1 \left(y_a - y_b \right) \times \delta(r + Vt - iL_s) + \sum_{j=1}^{m} F_j \delta\left(r - R_j \right) \Bigg\} dr = 0, \end{aligned} \tag{35}$$

$$\int_0^l W(r) \left\{ \begin{aligned} & \rho_a I_a \left(V^2 \frac{\partial^2 \varphi_a}{\partial r^2} - 2V \frac{\partial \varphi_a}{\partial r \partial t} + \frac{\partial^2 \varphi_a}{\partial t^2} \right) - E_a I_a \frac{\partial^2 \varphi_a}{\partial r^2} \\ & - k_a A_a G_a \frac{\partial y_a}{\partial r} + k_a A_a G_a \varphi_a \end{aligned} \right\} dr = 0. \tag{36}$$

Next, by adopting the Galerkin's method, the element mass, damping, and stiffness matrices of the moving rail beam element can be expressed as

$$\mathbf{M}_a^e = \rho_a A_a \int_0^l \mathbf{N}_{ay}^{\mathrm{T}} \mathbf{N}_{ay} dr + \rho_a I_a \int_0^l \mathbf{N}_{a\varphi}^{\mathrm{T}} \mathbf{N}_{a\varphi} dr, \tag{37}$$

$$\begin{aligned} \mathbf{C}_a^e = & -2\rho_a A_a V \int_0^l \mathbf{N}_{ay}^{\mathrm{T}} \mathbf{N}_{ay,r} dr - 2\rho_a I_a V \int_0^l \mathbf{N}_{a\varphi}^{\mathrm{T}} \mathbf{N}_{a\varphi,r} dr \\ & + c_1 \mathbf{N}_{ay}^{\mathrm{T}} \mathbf{N}_{ay} \delta\left(S_j \right) - c_1 \mathbf{N}_{ay}^{\mathrm{T}} \mathbf{N}_{by} \delta\left(S_j \right), \end{aligned} \tag{38}$$

$$\begin{aligned}\mathbf{K}_a^e &= \rho_a A_a V^2 \int_0^l \mathbf{N}_{ay}^{\mathrm{T}} \mathbf{N}_{ay,rr} dr + \rho_a I_a V^2 \int_0^l \mathbf{N}_{a\varphi}^{\mathrm{T}} \mathbf{N}_{a\varphi,rr} dr - E_a I_a \int_0^l \mathbf{N}_{a\varphi}^{\mathrm{T}} \mathbf{N}_{a\varphi,rr} dr \\ &\quad - k_a A_a G_a \int_0^l \mathbf{N}_{ay}^{\mathrm{T}} \mathbf{N}_{ay,rr} dr + k_a A_a G_a \int_0^l \mathbf{N}_{ay}^{\mathrm{T}} \mathbf{N}_{a\varphi,r} dr - k_a A_a G_a \int_0^l \mathbf{N}_{a\varphi}^{\mathrm{T}} \mathbf{N}_{ay,r} dr \\ &\quad + k_a A_a G_a \int_0^l \mathbf{N}_{a\varphi}^{\mathrm{T}} \mathbf{N}_{a\varphi} dr - c_1 V \mathbf{N}_{ay}^{\mathrm{T}} \mathbf{N}_{ay,r} \delta\left(S_j\right) + c_1 V \mathbf{N}_{ay}^{\mathrm{T}} \mathbf{N}_{by,r} \delta\left(S_j\right) \\ &\quad + k_1 \mathbf{N}_{ay}^{\mathrm{T}} \mathbf{N}_{ay} \delta\left(S_j\right) - k_1 \mathbf{N}_{ay}^{\mathrm{T}} \mathbf{N}_{by} \delta\left(S_j\right),\end{aligned} \tag{39}$$

where $(\ )_{,r}$ and $(\ )_{,rr}$ denote the first and second partial derivatives with respect to *r*, respectively; the terms containing the Dirac-delta function $\delta\left(S_j\right)$ are used to describe the effects of the motion of discrete rail pads.

For Eqs. (22) and (23), the corresponding moving track slab element matrices can be written as

$$\mathbf{M}_b^e = \rho_b A_b \int_0^l \mathbf{N}_{by}^{\mathrm{T}} \mathbf{N}_{by} dr + \rho_b I_b \int_0^l \mathbf{N}_{b\varphi}^{\mathrm{T}} \mathbf{N}_{b\varphi} dr, \tag{40}$$

$$\begin{aligned}\mathbf{C}_b^e &= -2\rho_b A_b V \int_0^l \mathbf{N}_{by}^{\mathrm{T}} \mathbf{N}_{by,r} dr - 2\rho_b I_b V \int_0^l \mathbf{N}_{b\varphi}^{\mathrm{T}} \mathbf{N}_{b\varphi,r} dr + c_1 \mathbf{N}_{by}^{\mathrm{T}} \mathbf{N}_{by} \delta\left(S_j\right) \\ &\quad - c_1 \mathbf{N}_{by}^{\mathrm{T}} \mathbf{N}_{ay} \delta\left(S_j\right) + c_2 \int_0^l \mathbf{N}_{by}^{\mathrm{T}} \mathbf{N}_{by} dr - c_2 \int_0^l \mathbf{N}_{by}^{\mathrm{T}} \mathbf{N}_{cy} dr,\end{aligned} \tag{41}$$

$$\begin{aligned}\mathbf{K}_b^e &= \rho_b A_b V^2 \int_0^l \mathbf{N}_{by}^{\mathrm{T}} \mathbf{N}_{by,rr} dr + \rho_b I_b V^2 \int_0^l \mathbf{N}_{b\varphi}^{\mathrm{T}} \mathbf{N}_{b\varphi,rr} dr - E_b I_b \int_0^l \mathbf{N}_{b\varphi}^{\mathrm{T}} \mathbf{N}_{b\varphi,rr} dr \\ &\quad - k_b A_b G_b \int_0^l \mathbf{N}_{by}^{\mathrm{T}} \mathbf{N}_{by,rr} dr + k_b A_b G_b \int_0^l \mathbf{N}_{by}^{\mathrm{T}} \mathbf{N}_{b\varphi,r} dr - k_b A_b G_b \int_0^l \mathbf{N}_{b\varphi}^{\mathrm{T}} \mathbf{N}_{by,r} dr \\ &\quad + k_b A_b G_b \int_0^l \mathbf{N}_{b\varphi}^{\mathrm{T}} \mathbf{N}_{b\varphi} dr + c_1 V \mathbf{N}_{by}^{\mathrm{T}} \mathbf{N}_{ay,r} \delta\left(S_j\right) - c_1 V \mathbf{N}_{by}^{\mathrm{T}} \mathbf{N}_{by,r} \delta\left(S_j\right) \\ &\quad + k_1 \mathbf{N}_{by}^{\mathrm{T}} \mathbf{N}_{by} \delta\left(S_j\right) - k_1 \mathbf{N}_{by}^{\mathrm{T}} \mathbf{N}_{ay} \delta\left(S_j\right) - c_2 V \int_0^l \mathbf{N}_{by}^{\mathrm{T}} \mathbf{N}_{by,r} dr \\ &\quad + c_2 V \int_0^l \mathbf{N}_{by}^{\mathrm{T}} \mathbf{N}_{cy,r} dr + k_2 \int_0^l \mathbf{N}_{by}^{\mathrm{T}} \mathbf{N}_{by} dr - k_2 \int_0^l \mathbf{N}_{by}^{\mathrm{T}} \mathbf{N}_{cy} dr,\end{aligned} \tag{42}$$

Similarly, the moving concrete base element matrices are given by

$$\mathbf{M}_c^e = \rho_c A_c \int_0^l \mathbf{N}_{cy}^{\mathrm{T}} \mathbf{N}_{cy} dr + \rho_c I_c \int_0^l \mathbf{N}_{c\varphi}^{\mathrm{T}} \mathbf{N}_{c\varphi} dr, \tag{43}$$

$$\mathbf{C}_c^e = -2\rho_c A_c V\int_0^l \mathbf{N}_{cy}^{\mathrm{T}}\mathbf{N}_{cy,r}dr - 2\rho_c I_c V\int_0^l \mathbf{N}_{c\varphi}^{\mathrm{T}}\mathbf{N}_{c\varphi,r}dr + c_2\int_0^l \mathbf{N}_{cy}^{\mathrm{T}}\mathbf{N}_{cy}dr$$
$$- c_2\int_0^l \mathbf{N}_{cy}^{\mathrm{T}}\mathbf{N}_{by}dr + c_3\int_0^l \mathbf{N}_{cy}^{\mathrm{T}}\mathbf{N}_{cy}dr, \tag{44}$$

$$\mathbf{K}_c^e = \rho_c A_c V^2\int_0^l \mathbf{N}_{cy}^{\mathrm{T}}\mathbf{N}_{cy,rr}dr + \rho_c I_c V^2\int_0^l \mathbf{N}_{c\varphi}^{\mathrm{T}}\mathbf{N}_{c\varphi,rr}dr - E_c I_c\int_0^l \mathbf{N}_{c\varphi}^{\mathrm{T}}\mathbf{N}_{c\varphi,rr}dr$$
$$- k_c A_c G_c\int_0^l \mathbf{N}_{cy}^{\mathrm{T}}\mathbf{N}_{cy,rr}dr + k_c A_c G_c\int_0^l \mathbf{N}_{cy}^{\mathrm{T}}\mathbf{N}_{c\varphi,r}dr - k_c A_c G_c\int_0^l \mathbf{N}_{c\varphi}^{\mathrm{T}}\mathbf{N}_{cy,r}dr \tag{45}$$
$$+ k_c A_c G_c\int_0^l \mathbf{N}_{c\varphi}^{\mathrm{T}}\mathbf{N}_{c\varphi}dr - c_2 V\int_0^l \mathbf{N}_{cy}^{\mathrm{T}}\mathbf{N}_{cy,r}dr + c_2 V\int_0^l \mathbf{N}_{cy}^{\mathrm{T}}\mathbf{N}_{by,r}dr$$
$$+ k_2\int_0^l \mathbf{N}_{cy}^{\mathrm{T}}\mathbf{N}_{cy}dr - k_2\int_0^l \mathbf{N}_{cy}^{\mathrm{T}}\mathbf{N}_{by}dr - c_3 V\int_0^l \mathbf{N}_{cy}^{\mathrm{T}}\mathbf{N}_{cy,r}dr + k_3\int_0^l \mathbf{N}_{cy}^{\mathrm{T}}\mathbf{N}_{cy}dr.$$

Upon assemblage of element matrices, the mass, damping and stiffness matrices of a typical moving track element can be written as

$$\mathbf{M}^e = \mathbf{M}_a^e + \mathbf{M}_b^e + \mathbf{M}_c^e, \tag{46}$$

$$\mathbf{C}^e = \mathbf{C}_a^e + \mathbf{C}_b^e + \mathbf{C}_c^e, \tag{47}$$

$$\mathbf{K}^e = \mathbf{K}_a^e + \mathbf{K}_b^e + \mathbf{K}_c^e, \tag{48}$$

Finally, by using the 'set-in-right-position' rule, the global mass matrix $\mathbf{M}_L$, damping matrix $\mathbf{C}_L$ and stiffness matrix $\mathbf{K}_L$ of the entire truncated slab track model can be obtained. The dynamic equations of motion of the slab track model can thus be written as

$$\mathbf{M}_L\ddot{\mathbf{Z}}_L + \mathbf{C}_L\dot{\mathbf{Z}}_L + \mathbf{K}_L\mathbf{Z}_L = \mathbf{F}_L, \tag{49}$$

where $\mathbf{Z}_L$ and $\mathbf{F}_L$ denote the displacement and force vectors of the slab track model, respectively.

5. System Equations and Numerical Solution

Eqs. (17) and (49) may be combined to obtain the coupled equations of motion of the vehicle-slab track system as follows

$$\begin{bmatrix}\mathbf{M}_U & \mathbf{0}\\ \mathbf{0} & \mathbf{M}_L\end{bmatrix}\begin{Bmatrix}\ddot{\mathbf{Z}}_U\\ \ddot{\mathbf{Z}}_L\end{Bmatrix} + \begin{bmatrix}\mathbf{C}_U & \mathbf{0}\\ \mathbf{0} & \mathbf{C}_L\end{bmatrix}\begin{Bmatrix}\dot{\mathbf{Z}}_U\\ \dot{\mathbf{Z}}_L\end{Bmatrix} + \begin{bmatrix}\mathbf{K}_U & \mathbf{0}\\ \mathbf{0} & \mathbf{K}_L\end{bmatrix}\begin{Bmatrix}\mathbf{Z}_U\\ \mathbf{Z}_L\end{Bmatrix} = \begin{Bmatrix}\mathbf{F}_U\\ \mathbf{F}_L\end{Bmatrix}, \tag{50}$$

which may be solved in the time domain using Newmark’s constant acceleration scheme. To ensure the accuracy of the results, the time step is controlled within 0.0001s.[16] In view of the fact that the force vector contains nonlinear terms describing the wheel-rail interaction, Newton-Raphson’s scheme is used to iteratively linearize the equations at each time step, and the convergence tolerance of rail displacement at wheel-rail contact points is controlled not to exceed 1.0×10^{-5}.[32]

6. Numerical Validation

The numerical simulation based on the proposed model is conducted using MATLAB. The accuracy of the results is validated through comparison with available results in the open literature.[22,35]

The first validation study is made by comparing with the FEST results by Lei and Wang[22], in which the dynamic response of the CRTSII slab track when a CRH3 vehicle passes by at a speed of 72 km/h was analyzed. The vehicle characteristics and slab track properties used in the study are given in Tables 1 and 2, respectively. Note that there is no track irregularity and the wheel-rail interaction is assumed linear.[22]

The computed vertical rail displacements and wheel-rail contact force are presented in Figs. 3 and 4, respectively. As illustrated in Fig. 3, a very good match of the steady-state rail displacement is observed between the proposed model and the results by Lei and Wang[22] despite that some minor discrepancies are observed at the contact points between the rail and the front and rear wheel-sets. Fig. 4 shows the time history results of the wheel-rail contact force as the vehicle moves over a distance of 70 m. The results obtained using the proposed model generally agree well with those reported in the literature. The difference is that the wheel-rail contact force history curve obtained using the present model is not a smooth curve, but has small and dense oscillations. These oscillations may be attributed to the parameter excitation caused by the discrete rail pads, which is similar to the periodic vibration caused by the discrete sleepers of ballasted tracks.[36] However, such oscillations are not observed in the results by Lei and Wang[22], owing to the fact that the rail is assumed to be continuously supported by the substructure in their study. From the comparison displayed in Figs. 3 and 4, it is also obvious that the effect of discrete rail pads on rail displacement is less than that on the contact force.

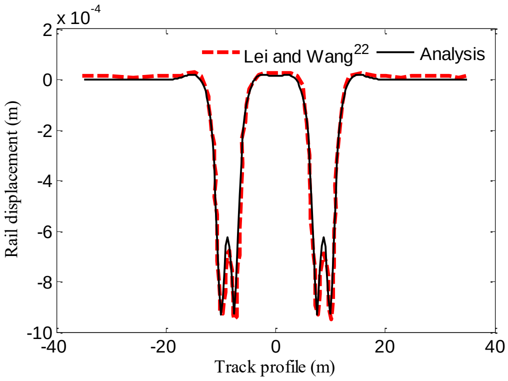

Fig. 3. Rail displacement profile.

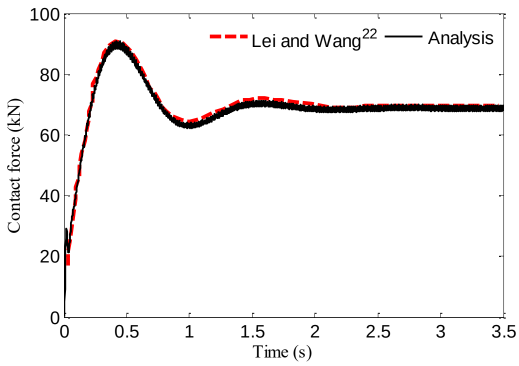

Fig. 4. Wheel-rail contact force history.

Table 1. Parameters for Chinese high-speed train CRH3[32]

Parameters	Value
Mass of coach body 2 m_v (kg)	40,000
Mass of bogie 2 m_t (kg)	3200
Mass of wheel m_w (kg)	1200
Pitch inertia of vehicle body 2 J_v (kg·m^2)	5.47×10^5
Pitch inertia of vehicle body 2 J_t (kg·m^2)	6800
Stiffness of primary suspension system 2 k_{s1} (MN/m)	2.08
Stiffness of secondary suspension system 2 k_{s2} (MN/m)	0.8
Damping of primary suspension system 2 c_{s1} (kN·s /m)	100
Damping of secondary suspension system 2 c_{s2} (kN·s /m)	120
Wheelbase 2 l_1 (m)	2.50
Distance between centers of front and rear bogies 2 l_2 (m)	17.375
Stiffness of wheel-rail contract k_c (MN/m)	1.325×10^3
Axle load (kN)	140

Table 2. Parameters for CRTSII slab track[32]

Parameters		Value
Rail pad	Distance of ties (m)	0.625
	Stiffness of pad ($MN \cdot m^{-1}$)	60
	Damping of pad ($kN \cdot s \cdot m^{-1}$)	50
Track slab	Length (m)	6.45
	Width (m)	2.55
	Height (m)	0.20
	Density ($kg \cdot m^{-3}$)	2500
	Young's modulus (MPa)	3.9×10^4
Cement-asphalt layer	Stiffness ($MN \cdot m^{-1}$)	0.9×10^3
	Damping ($kN \cdot s \cdot m^{-1}$)	80
Concrete base	Upper bottom width (m)	2.95
	Lower bottom width (m)	3.25
	Height (m)	0.30
	Density ($kg \cdot m^{-3}$)	2500
	Young's modulus (MPa)	3.3×10^4
Subgrade	Stiffness ($MN \cdot m^{-1}$)	65
	Damping ($kN \cdot s \cdot m^{-1}$)	90

To further examine the accuracy of the proposed model, the vertical vehicle-track dynamic interaction investigated by Aggestam et al.[35] is considered. In their study, two slab track models, namely a two-layer Timoshenko beam model and a three-layer Timoshenko beam model, were employed in combination with an extended state-space vector and a complex-valued modal superposition. In both models, the rail pads were modelled as discrete elastic point supports spaced uniformly apart at 0.65 m. Based on the model presented in this paper, the static stiffness of the rail along the longitudinal direction is estimated based on the properties reported.[35] Fig. 5 shows the static stiffness of the rail evaluated by the present model and that reported by Aggestam et al. As can be seen, both models agree well with each other, thereby validating the applicability of the proposed model.

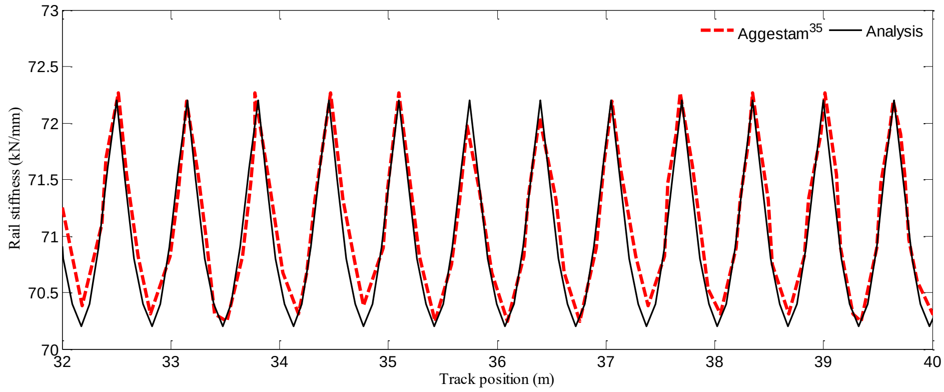

Fig. 5. Rail static stiffness.

Next, we compare the dynamic wheel-rail contact force of the coupled system. It should be noted that the 10-DOF vehicle model adopted in this study is reduced to a 4-DOF model.[35] Also note that a low-pass filter technique was applied to eliminate the oscillations in the wheel-rail contact force due to the finite element interpolation polynomials used for Timoshenko beam elements.[31,35] Although the MEM model does not encounter the motion of load points, the motion of the discrete supports relative to the rail beam also introduces some spurious fluctuations in the results. Therefore, the Butterworth low-pass filter[37] is employed to filter out these spurious fluctuations. Fig. 6 shows the steady-state wheel-rail contact force when the vehicle speed is 100 km/h. It can be seen that although there are some differences between the current and reported results, the maximum difference in contact force amplitude is less than 1%. The dynamic wheel-rail contact force experiences periodic variations. This is due to the periodic excitation caused by the discrete rail pads which would not be observed for the case of continuously supported rails, as shown in the results by Lei and Wang[22] in Fig. 4.

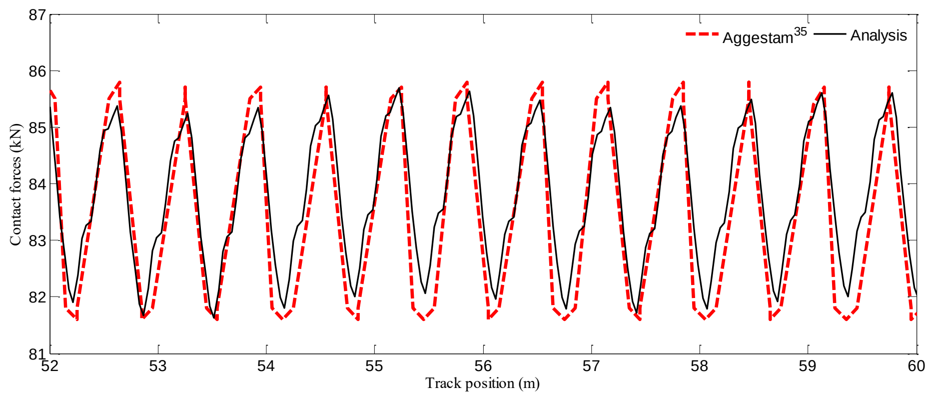

Fig. 6. Wheel-rail contact force at steady state with low-pass filter.

7. Dynamic Response of Train-Slab Track System

In this section, a parametric study is carried out to find out the effects of vertical track irregularity and train speed on the dynamic responses of the CRH3 vehicle traversing the CRTSII slab track system supported on discrete rail pads. The vehicle characteristics and slab track properties specified earlier in Tables 1 and 2 are employed. In the following analysis, the track segment between two adjacent rail pads is discretized into 4 elements, and the total length of the track model is set to 140 m.

As is well-known, the response of the coupled train-track system is significantly affected by the severity of the track irregularity. The cause of track irregularity may be due to track formation technology, wear, clearances, settlement, and other factors. The most common type of track irregularity is due to rail wear and weld defects, with wavelengths ranging from a few centimeters to about 3 meters.[17] For track irregularities with larger wavelengths, its formation is often related to the track structure and its foundation.[38-39] There are generally two approaches to describe track irregularity, namely deterministic functions and stochastic processes.[16,22,40-42] Here, a sinusoidal function to represent the track irregularity in the vertical profile is adopted, which can be written as

$$y_t = A\sin\left(2\pi x / B\right), \tag{51}$$

where A and B denote the amplitude and wavelength of the rail irregularity, respectively.

Figs. 7 and 8 show the time history of the rail displacement at the contact point under wheel 1. Two different track irregularity wavelengths of 0.5 m and 1.0 m and four amplitudes of 0 (smooth track), 0.1 mm, 0.3 mm and 0.5 mm are considered. The vehicle travels at a speed of 72 km/h. With the same irregularity wavelength, the rail displacement under the contact point increases significantly as the amplitude of irregularity increases. Comparatively speaking, with the same irregularity amplitude, when the wavelength changes from 0.5 m to 1.0 m, the periodic change of track displacement is obvious, but in terms of the dynamic rail displacement amplitude, the change is insignificant. In addition, one can also find that when the track irregularity is not considered (i.e., amplitude is 0), the rail displacement experiences small periodic variations due to the discrete rail pads.

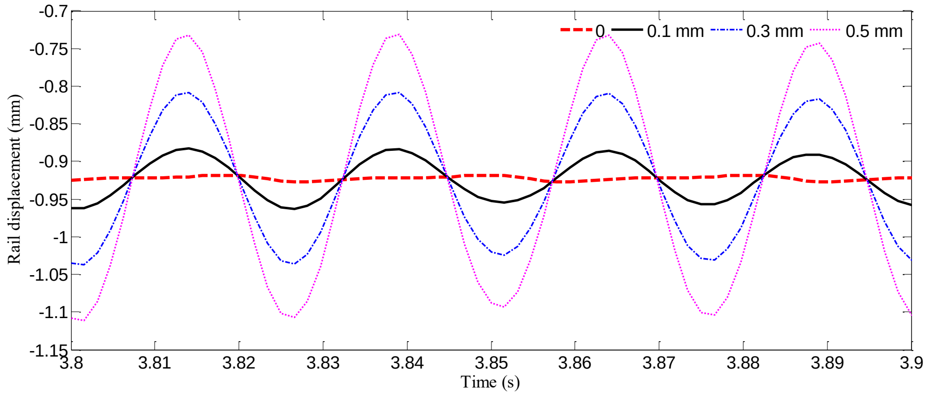

Fig. 7. Rail displacement at contact point of wheel 1.
(V=72 km/h, wavelength=0.5 m, amplitude=0, 0.1, 0.3, 0.5 mm)

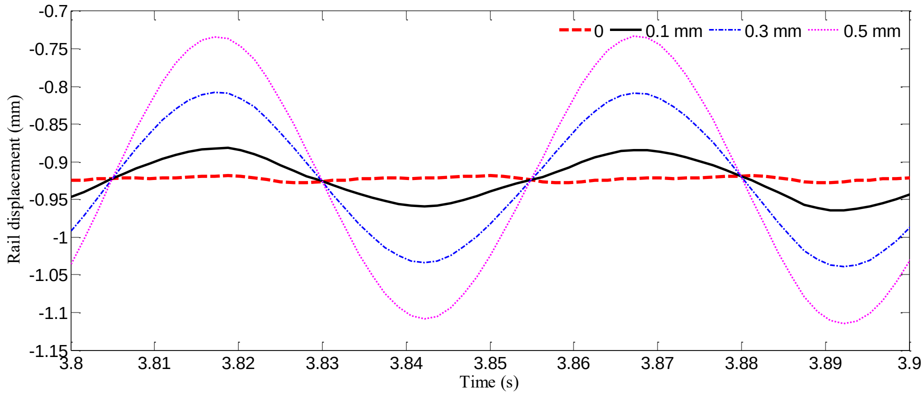

Fig. 8. Rail displacement at contact point of wheel 1.
(*V*=72 km/h, wavelength=1.0 m, amplitude=0, 0.1, 0.3, 0.5 mm)

Figs. 9-10 show the time history of the wheel-rail contact force developed at wheel 1. Clearly, the amplitude of track irregularity is the key factor causing the amplification of the wheel-rail contact force. By comparing Fig. 9 with Fig. 10, it is observed that as the irregularity wavelength becomes shorter, the periodic change of the wheel-rail contact force is prominent, and its magnitude increases significantly. It may be concluded that the irregularity wavelength also has a significant effect on the wheel-rail contact force. It is interesting to note that with the aggravation of rail irregularity, i.e. shorter wavelength and/or larger amplitude, the periodic oscillation of wheel-rail contact force appears to vanish, which can be attributed to the relatively larger "roughness excitation".[43-44]

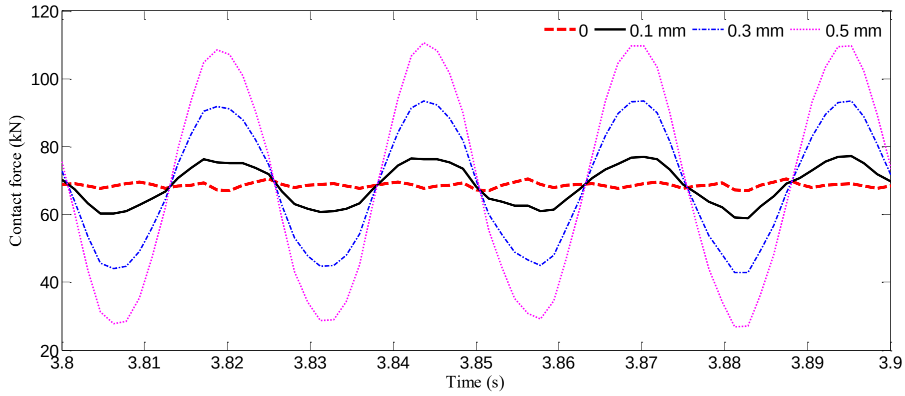

Fig. 9. Wheel-rail contact force at contact point of wheel 1.
(*V*=72 km/h, wavelength=0.5 m, amplitude=0, 0.1, 0.3, 0.5 mm)

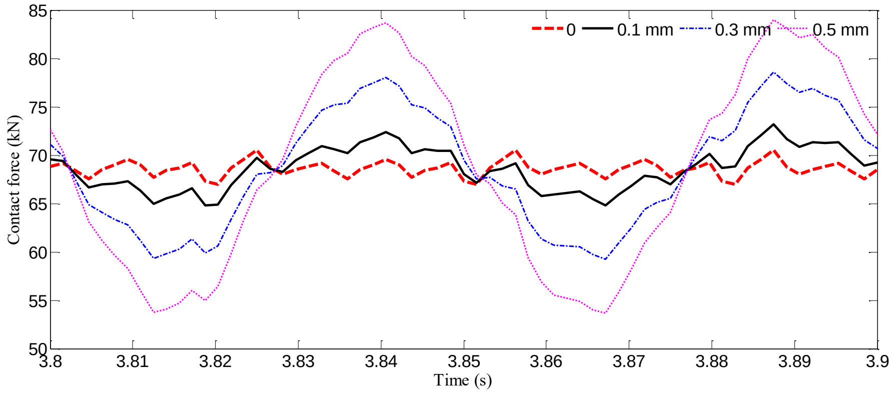

Fig. 10. Wheel-rail contact force at contact point of wheel 1.
(*V*=72 km/h, wavelength=1.0 m, amplitude=0, 0.1, 0.3, 0.5 mm)

To study the effect of vehicle speed on the coupled system, the peak displacement and acceleration responses of the track are investigated. Five different speeds, namely 160 km/h, 200 km/h, 250 km/h, 300 km/h and 350 km/h, are considered. In the following analysis, the wavelength of the track irregularity is kept at 1.0 m, but three different amplitudes of 0.0 mm, 0.1 mm and 0.3 mm are considered.

Fig.11 presents the effect of vehicle speed on the peak displacement and acceleration of the rail. When the vehicle speed increases from 160 km/h to 350 km/h, the changes in the rail displacement and acceleration are expectedly insignificant for the case of a smooth railhead. With the increase of the irregularity amplitude, the peak displacement and acceleration of the rail increase substantially. When the degree of track irregularity is large, the effect of vehicle speed on rail acceleration is stronger than that on displacement. Moreover, the increase is noted to be not monotonous with the increase in speed. For example, the peak acceleration of the rail reaches its maximum value of 1120 m/s^2 at a speed of 250 km/h. This may be due to the fact that the excitation frequency is close to the natural frequency of the train-track system at a speed of 250 km/h, leading to a much amplified acceleration response. Figs.12 and 13 also present the peak displacement and peak acceleration of the track slab and concrete base, respectively. It can be seen from Fig. 13 that the displacement and acceleration of the concrete base also do not increase monotonously with the vehicle speed. The peak displacement and acceleration are only -0.63 mm and 37 m/s^2, respectively. Compared to the rail beam, the displacement and acceleration responses of the track slab and concrete base are much smaller. This is expected in view of the damping effects of each sub-structure of the coupled system.

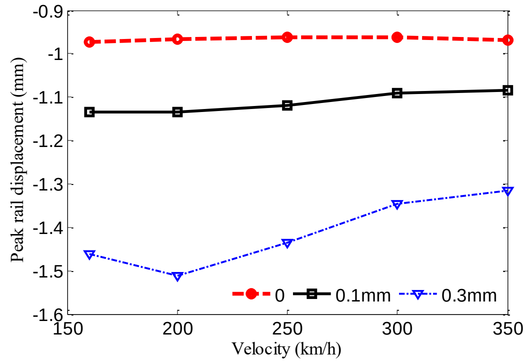

(a) Displacement

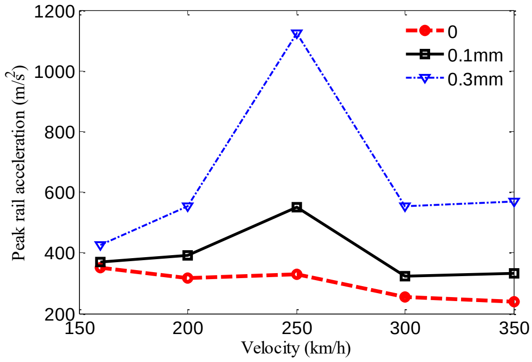

(b) Acceleration

Fig. 11. Peak displacement and acceleration of rail beam.
(wavelength=1.0 m, amplitude=0, 0.1, 0.3 mm)

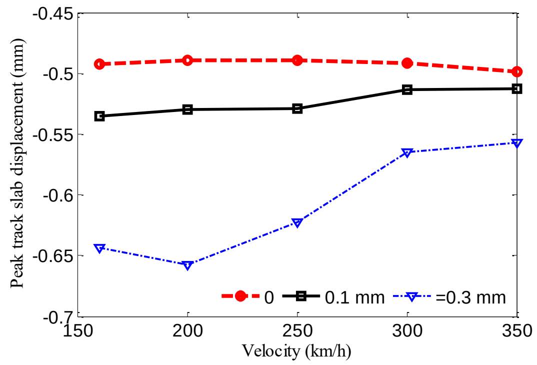

(a) Displacement

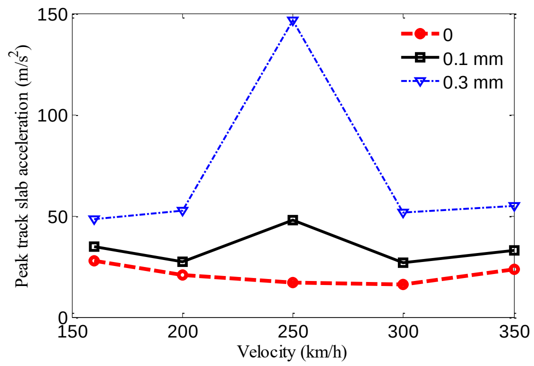

(b) Acceleration

Fig. 12. Peak displacement and acceleration of track slab.
(wavelength=1.0 m, amplitude=0, 0.1, 0.3 mm)

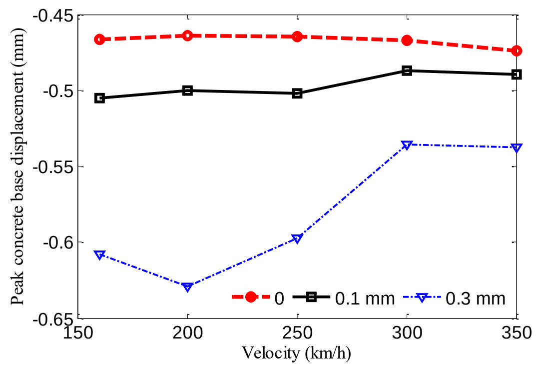

(a) Displacement

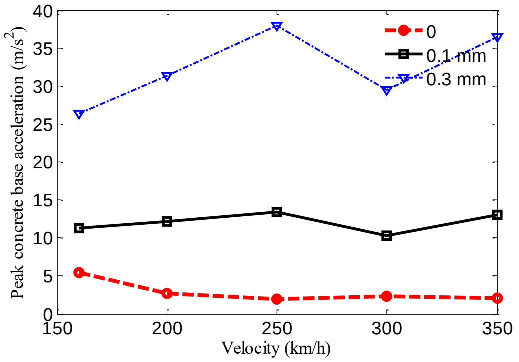

(b) Acceleration

Fig. 13. Peak displacement and acceleration of concrete base.
(wavelength=1.0 m, amplitude=0, 0.1, 0.3 mm)

Fig.14 presents the variation of the peak wheel-rail contact force of wheel 1 with respect to the vehicle speed. When the track is perfectly smooth, the maximum wheel-rail contact force is almost unaffected by the vehicle speed. The severity of the track irregularity has a significant amplification effect on the contact force. As the vehicle speed increases, this amplification effect does not increase monotonically with the vehicle speed. When the speed is 250 km/h, the wheel-rail contact force reaches the maximum value, which is about 1.7 times the half static axle weight. To explain this phenomenon, we further compared the contact forces of the four wheel-sets during a period of time under steady-state vibration, as shown in Fig. 15. Obviously, due to the presence of the track irregularity, two contact forces developed at the two wheel-sets under the same bogie, i.e. wheels 1 and 2, present an alternate oscillation. More specifically, when the contact force at wheel 1 is the largest, the contact force at wheel 2 reaches its minimum value; on the contrary, when the contact force at wheel 1 is the smallest, the contact force at wheel 2 reaches its maximum value. The same applies to the contact forces developed at wheels 3 and 4.

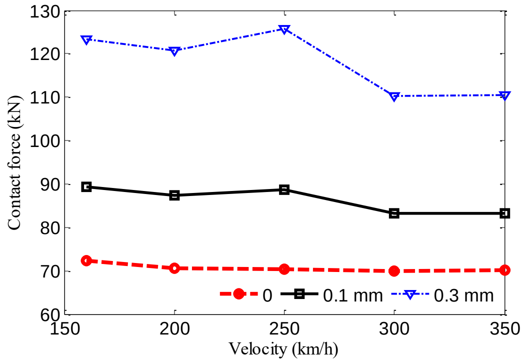

Fig. 14. Peak contact force of wheel 1.
(wavelength=1.0 m, amplitude=0, 0.1, 0.3 mm)

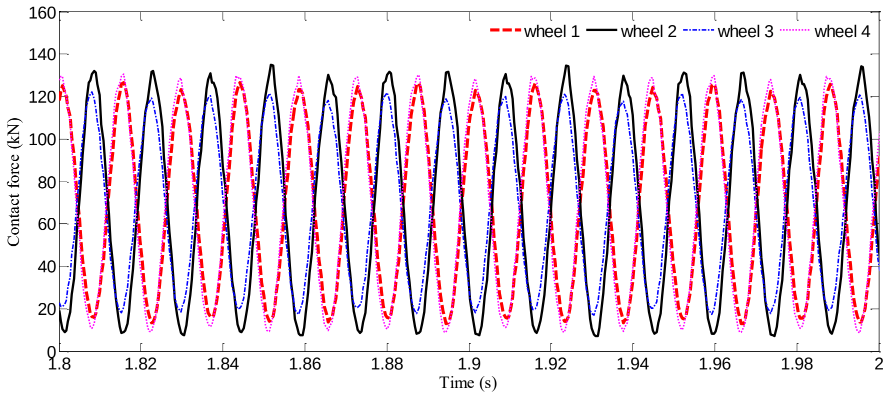

Fig. 15. Wheel-rail contact forces of wheels 1, 2, 3, 4
(V=250 km/h, wavelength=1.0 m, amplitude= 0.3 mm)

Finally, the effect of the vehicle speed on the vertical acceleration of the coach is investigated for the case of track irregularity wavelength of 1.0 m. As can be seen from Fig.16, the amplitude of the irregularity has almost no effect on the peak vertical acceleration of the coach. In addition, as the speed of the vehicle increases, the vertical acceleration response of the coach is very small, and the maximum acceleration is less than 0.09 m/s^2. It may be concluded that the primary and secondary suspension systems of the CRH3 have a good damping effect on the vibration of the coach thus leading to a high comfort level for the passengers.

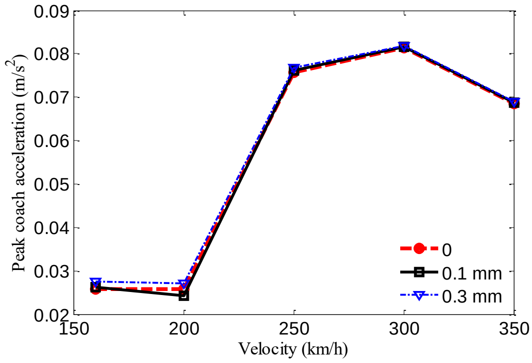

Fig. 16. Peak coach acceleration.
(wavelength=1.0 m, amplitude=0, 0.1, 0.3 mm)

8. Conclusion

A new three-layer Timoshenko beam model with discrete rail pads is proposed for the railway slab track. A computational scheme based on the MEM is proposed for the study of an infinitely long slab track with viscously damped elastic supports. The dynamic response of the high-speed train-slab track system is investigated, in which the train is modelled as a moving 10-DOF multi-body and the coupling between the vehicle and track is established by considering the nonlinear contact between the wheel and the rail. The proposed method is shown to be an effective and accurate approach for the analysis of high-speed train-slab track systems.

A realistic modelling technique for discrete rail pads is presented. Studies considering the evenly spaced discrete rail pads are carried out to investigate the dynamic responses of the system. Results show that the periodic static stiffness variation arising from the discretely supported pads will generate an excitation on the moving vehicle at the pad passing frequency and thus cause dynamic vibrations even when the railhead is perfectly smooth. It is thus important to consider the effects of discrete rail pads in the slab track model.

The influence of short harmonic track irregularities on the dynamic response of the system is investigated. The results show that the irregularity amplitude has a significant effect on the dynamic wheel-rail contact force. For the effect of irregularity wavelength, the situation is more complicated, as it depends on the static stiffness changes caused by the discrete rail pads, the frequency of excitations by irregularity, the vehicle speed, and the natural frequencies of the coupled vehicle-track system.

The effect of different vehicle speeds on the peak displacement, acceleration, and wheel-rail contact force of the vehicle-track system is also examined. If the railhead is smooth, the vehicle speed has a negligible effect on the dynamic response of the system.

However, the vehicle speed substantially amplifies the dynamic response of the system, especially the wheel-rail contact force and rail acceleration, in cases of short harmonic track irregularities. Moreover, this effect does not increase monotonically with the vehicle speed. In addition, the maximum coach body acceleration is found to be small for all vehicle speeds considered in the study.

Although the MEM eliminates the need to track the wheel-rail contact points and assigns contact forces to element nodes that are superior to the conventional FEM, the motion of discrete rail pads however introduces some similar complications encountered by the FEM. To further improve the accuracy and reduce the spurious wheel-rail force oscillations in the numerical results, a refined mesh of the slab track may be needed.

Acknowledgments

This work has been supported by the Natural Science Foundation of China (Grant no.51578072, 51578077). The authors are grateful for these supports.

References

1. C. Esveld, Recent developments in high-speed track, *Eur. Railw. Rev.* **9**(2) (2003) 81–85.
2. J. J. Yang, S. Y. Zhu and W. M. Zhai, Modeling slab track for vehicle-track-coupled dynamics analysis using spline function method, *Int. J. Struct. Stab. Dyn.* **20**(2) (2020) 1-28.
3. L. Frýba, *Vibration of solids and structures under moving loads* (Thomas Telford, London, 1999).
4. M. H. Kargarnovin and D. Younesian, Dynamics of Timoshenko beams on Pasternak foundation under moving load, *Mecha. Res. Comm.* **31**(2004) 713-723.
5. S. M. Kim, Stability and dynamic response of Rayleigh beam-columns on elastic foundation under moving loads of constant amplitude and harmonic variation, *Eng. Struct.* **27**(2005) 869-880.
6. C. W. Cai, Y. K. Cheung and H. C. Chan, Dynamic response of infinite continuous beams subjected to a moving force-an exact method, *J. Sound Vib.* **123**(3) (1988) 461-472.
7. N. Azizi, M. M. Saadatpour and M. Mahzoon, Using spectral element method for analyzing continuous beams and bridges subjected to a moving load, *Appl. Math. Model.* **36** (2012) 3580-3592.
8. F. V. Filho, Finite element analysis of structures under moving loads, *Shock Vib. Dig.* **10** (1978) 27-35.
9. M. Esmaeili, S. Mohammadzadeh and M. Mehrali, Dynamic response of the coupled vehicle-floating slab track system using finite element method, *Int. J. Transp. Eng.* **4**(1) (2016) 9-26.
10. X. Y. Lei and B. Zhang, Analysis of dynamic behavior for slab track of high-speed railway based on vehicle and track element. *J. Transp. Eng.* **137**(4) (2011) 227-240.
11. W. M. Zhai, K. Y. Wang and C. B. Cai, Fundamentals of vehicle-track coupled dynamics, *Veh. Syst. Dyn.* **47**(11) (2009) 1349-1376.
12. Q. Y. Xu, B. Li and X. L. Zhou, Dynamic coefficient of slab track system on subgrade under high-speed trains, *J. Cen. South. Univ.* (*Sci. Tech.*) **42**(9) (2011) 2831-2836.
13. C. Vale and R. Calcada, A dynamic vehicle-track interaction model for predicting the track degradation process, *J. Infrastruct. Syst.* **20**(3) (2014) 1-13.
14. S. Krenk, L. Kellezi, S. R. K. Nielsen and P. H. Kirkegaard, Finite elements and transmitting boundary conditions for moving loads, in *Proc. 4th European Conf. on Structural Dynamics, Eurodyn '99*, Praha (A.A./Taylor & Francis, The Netherlands, 1999), 447–452.
15. L. Andersen, S. R. K. Nielsen and P. H. Kirkegaard, Finite element modeling of infinite Euler beams on Kelvin foundations exposed to moving loads in convected co-ordinates, *J. Sound Vib.* **241** (4) (2001) 587-604.
16. C. G. Koh, J. S. Y. Ong, D. K. H. Chua, and J. Feng, Moving element method for train-track dynamics, *Int. J. Numer. Meth. Engng.* **56** (2003) 1549-1567.
17. K. K. Ang and J. Dai, Response analysis of high-speed rail system accounting for abrupt change of foundation stiffness, *J. Sound Vib.* **332** (2013) 2954-2970.

18. M. T. Tran, K. K. Ang, V. H. Luong and J. Dai, High-speed trains subject to abrupt braking, *Veh. Syst. Dyn.* **54** (2016) 1715-1735.
19. J. Dai, M. Han and K.K. Ang, Moving element analysis of partially filled freight trains subject to abrupt braking, *Int. J. Mech. Sci.* **151** (2019) 85-94.
20. J. Dai, K. K. Ang, M. T. Tran, V. H. Luong and D. Jiang, Moving element analysis of discretely supported high-speed rail system, *Proc. Inst. Mech. Eng. Pt. J: Rail Rapid Transit*. **232**(3) (2018) 783–97.
21. J. Dai, K. K. Ang, D. Jiang, V. H. Luong and M. T. Tran, Dynamic response of high-speed train-track system due to unsupported sleepers, *Int. J. Struct. Stab. Dyn.* **18**(10) (2018) 1850122.
22. X. Y. Lei and J. Wang, Dynamic analysis of the train and slab track coupling system with finite elements in a moving frame of reference, *J. Vib. Control.* **20**(9) (2014) 1301-1317.
23. V. H. Luong, T. N. T. Cao, Q. X. Lieu and X. V. Nguyen, Moving element method for dynamic analyses of functionally graded plates resting on Pasternak foundation subjected to moving harmonic load, *Int. J. Struct. Stab. Dyn.* **20**(1) (2020) 1-25.
24. V. H. Luong, T. N. T. Cao, J. N. Reddy, K. K. Ang, M. T. Tran and J. Dai, Static and dynamic analyses of Mindlin plates resting on viscoelastic foundation by using moving element method, *Int. J. Struct. Stab. Dyn.* **18**(11) (2018) 1-20.
25. J. Dai, K. K. Ang, V. H. Luong, M. T. Tran and D. Q. Jiang, Out-of plane responses of overspeeding high-speed train on curved track, *Int. J. Struct. Stab. Dyn.* **18**(11) (2018) 1850132.
26. X. V. Nguyen, V. H. Luong, T. N. T. Cao, X. Q. Lieu and T. B. Nguyen, Hydroelastic responses of floating composite plates under moving loads using a hybrid moving element-boundary element method, *Adv. Struct. Eng.* **00**(0) (2020) 1-17.
27. V. H. Luong, X. V. Nguyen, T. N. T. Cao, M. T. Tran and H. P. Nguyen, A time-domain 3D BEM-MEM method for flexural motion analyses of floating Kirchhoff plates induced by moving vehicles, *Int. J. Struct. Stab. Dyn.* **20**(2) (2020) 2050041.
28. J. N. Reddy, X. V. Nguyen, T. N. T. Cao, Q. X. Lieu and V. H. Luong, An integrated moving element method (IMEM) for hydroelastic analysis of infinite floating Kirchhoff-Love plates under moving loads in a shallow water environment, *Thin Wall. Struct.* **155** (2020) 106934.
29. K. Knothe, Z. Strzyzakowski and K. Willer, Rail vibrations in the high frequency range, *J. Sound Vib.* **169**(1) (1994) 111-123.
30. Z. S. Xu, W. M. Zhi, K. Y. Wang and Q. C. Wang, Analysis of vehicle-track system vibration: comparison between Timoshenko beam and Euler beam track model, *EARTHQ. ENG. ENG. VIB.* **23**(6) (2003) 74-79.
31. B. Blanco, A. Alonso, L. Kari, N. Gil-Negrete and J. G. Gimenez, Implementation of Timoshenko element local deflection for vertical track modelling, *Veh. Syst. Dyn.* **57**(10) (2019) 1421-1444.
32. X. Y. Lei, S. H. Wu and B. Zhang, Dynamic analysis of the high speed train and slab track nonlinear coupling system with the cross iteration algorithm, *J. Nonlin. Dyn.* **2016** (2016) 8356160.
33. W. M. Zhai, *Vehicle-track coupled dynamics* (Science Press, Beijing, 2020).
34. J. N. Reddy, On locking-free shear deformable beam finite elements, *Comput. Methods Appl. Mech. Eng.* **149** (1997) 113-132.
35. E. Aggestam, J. C. O. Nielsen and R. Bolmsvik, Simulation of vertical dynamic vehile-track interaction using a two-dimensional slab track model, *Veh. Syst. Dyn.* **56**(11) (2018) 1633-1657.
36. T. X. Wu and D. J. Thompson, On the parametric excitation of the wheel/track system, *J. Sound Vib.* **278** (2004) 725-747.
37. MathWorks, Butterworth filter design-Matlab butter [cited May 1, 2020], available from: https://www.mathworks.com/help/signal/ref/butter.html.
38. M. PODWORNA, Modelling of random vetical irregularities of railway tracks, *Int. J. Appl. Mech. Eng.* **20**(3) (2015) 647-655.
39. S. L. Grassie and J. Kalousek, Rail corrugation: characteristics, causes and treatments, *Proc. Inst. Mech. Eng. Pt. F: Rail Rapid Transit.* **207**(1) (1993) 57-68.
40. X. Y. Lei and N. A. Noda, Analysis of dynamic response of vehicle and track coupling system with random irregularity of track vertical profile, *J. Sound Vib.* **258**(1) (2002) 147-165.
41. G. Y. Tian, J. M. Gao and C. F. Zhao, Progress in the research on the railway track irregularity power spectral density, *J. Railw. Eng. Soc.* **216**(9) (2016) 35-40,81.
42. S. L. Grassie, R. W. Gregory, D. Harrison and K. L. Johnson, The dynamic response of railway track to hight frequency vertical excitation, *J. Mech. Eng. Sci.* **24**(2) (1982) 77-90.
43. S. C. Yang, Enhancement of the finite-element method for the analysis of vertical train-track interactions,

Proc. Inst. Mech. Eng. Pt. J Rail Rapid Transit. **223**(6) (2009) 609-620.
44. J. C. O. Nielsen and A. Igeland, Vertical dynamic interaction between train and track-influence of wheel and track imperfections, *J. Sound Vib.* **187**(5) (1995) 825-839.